Pure

Scotland's Rural College

Dual role of 2-aminodiphenylamine with graphene oxide-palladium supported catalyst for direct methanol fuel cell application and removal of Otto fuel II component

Mishra, Kirti; Devi, Nishu; Siwal, Samarjeet Singh; Thakur, Vijay Kumar

Link to publication

Dual role of 2-aminodiphenylamine with graphene oxide-palladium supported catalyst for direct methanol fuel cell application and removal of Otto fuel II component

Kirti Mishra [a], Nishu Devi [b], Samarjeet Singh Siwal [a,c,*], Vijay Kumar Thakur [c,*]

[a] *Department of Chemistry, M.M. Engineering College, Maharishi Markandeshwar (Deemed to be University), Mullana-Ambala, Haryana, 133207, India*
[b] *Mechanics and Energy Laboratory, Department of Civil and Environmental Engineering, Northwestern University, 2145 Sheridan Road, Evanston, IL60208, USA*
[c] *Biorefining and Advanced Materials Research Center, SRUC, Kings Buildings, West Mains Road, Edinburgh EH9 3JG, UK*

ABSTRACT

For the first time, we describe the synthesis of Pd nanoparticles (Pd(0)) using 2-aminodiphenylamine (2*ADPA*) with graphene oxide as support. Furthermore, we incorporated the Pd(0)-2*ADPA,* which was enriched with graphene oxide and used to modify a glassy carbon electrode surface. We used this catalyst as the methanol oxidation reaction (MOR) in the alkaline media shows good catalytic behavior within the fuel cell application and removal of the Otto fuel II component. Several characterizations evidence the successful formation of Pd(0)-2*ADPA* by spectroscopic and optical techniques. We have studied the reduction reaction of the 2-nitrodiphenyl-amine (2-NDPA) to investigate the catalytic performance of the synthesized material. We used various electro-chemical methods, for example, chronoamperometry (CA) and cyclic voltammetry (CV) and electrochemical impedance spectroscopy (EIS), to review the stability of our proposed catalyst. The stability of the Pd electro-catalyst was improved by covering it with 2*ADPA*. The incorporated Pt-free electrocatalyst is incredibly favorable for facilitating the direct methanol fuel cell cost due to the incorporation of conductive polymer support material.

1. Introduction

As the energy requirement and environmental concerns are increasing, fossil fuels are not an excellent long-term origin of energy any more. Necessary actions and analyses have been turned to renew-able power production and or power authorities [1–3]. Fuel cells (FCs) have attracted recognition as a clean, renewable energy source for mobile tools, electric carriers and on-the-spot power production pro-cesses with high energy efficacy and low fatigue levels. However, price and stability problems have hindered its large-scale commercialization [4–6]. A FC consists mainly of an anode traditionally supplied hydrogen and a cathode to which oxygen is provided, detached through an elec-trolyte. Gaseous hydrogen as an oxidant has newly been substituted by liquid oxidants (fuels) that are of higher energy and higher density and have more ease of transport, storage, handling and processing [7–9].

Low molecular weight alcohol fuels such as methanol (MeOH), ethanol, and propanol, ethylene glycol are the most appropriate fuels for a direct alcohol FC (DAFC) because of their simple structure, high energy density and low molecular weights [10–12]. MeOH used as the primary

fuel in this study is considered since it can be directly fed into a reactor without reformation and is produced from different roots like natural gas, oil, coal or biomass. MeOH oxidation, in particular, has reported higher activity in basic media than in acidic media. Alkaline MeOH FCs have reported better oxygen reduction kinetics and comparable effi-ciencies [13]. Direct methanol FCs (DMFCs) may reduce catalyst loading and, therefore, the application of cheap non-precious metal catalysts [14]. The overall oxidation of MeOH involves the release of six electrons and a water molecule, as illustrated in Eq. (1). The performance of the alcohol FC (AFC) is improved by the recirculation of the electrolyte and the continuous removal of CO_2, which may prevent significant carbon-ation poisoning [7].

$$CH_3OH + 6OH^- \rightarrow CO_2 + 5H_2O + 6e^- \qquad (1)$$
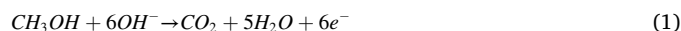
The support material interaction may contribute to stabilizing the metal particles and their associated activity (i.e., may increase or decrease it). The support's interaction with poisonous species, such as CO, during MeOH oxidation, may impair the activity of the FC [15]. Palladium, however, has been demonstrated to have the power to

overcome protons, stock and liberation hydrogen and further eliminate adsorbed CO from the MeOH electro-oxidation, reducing the poisoning impact [16]. This decline is achieved by palladium during its release of hydrogen, which provides a way for reducing the surface concentration of the adsorbed CO, therefore, the constant oxidation of organic molecules at the palladium surface [17–19]. Graphitic carbon nitride is quite a popular metal-free heterogeneous catalyst. The material attracts interest due to its various active centers and high chemical and thermal stability. It may be an efficient heterogeneous catalyst or a good co-catalytic support [20–22].

Thus, DMFC is a promising technology to include in the dynamic market; for example, it can simply be introduced into the administration network. The core problems are still the progress of anodes with better performance. Currently, the anode includes a high storing of noble metals (e.g., Pt and Pd), and its kinetic is considerably slow. Hence, the main jobs of low-temperature FC catalytic technology are growing economy materials with high catalytic activity and high stability in a highly corrosive factor. Another way to improve platinum's catalytic performance is to use catalyst support. The environment of the support can change the size, shape and pattern of the platinum nanoparticles, leading to a modification of the number and nature of existing sites, which could significantly modify the catalytic performance of the catalyst. The support may give synergetic outcomes, changing the electronic features of the operating sites, which influences the adsorption power of molecules on the surface and, consequently, the reactivity [23,24].

In specific apparatuses, Pt/carbon materials are used as electrode materials towards chemical energy improvement of fuel to electricity via electrocatalytic reactions, for example, methanol oxidation reaction (MOR) at the anodes of DMFCs and oxygen reduction reaction (ORR) at the cathodes of PEMFCs [25]. Liquid FCs, covering MeOH FCs and formic acid FCs, are known to inspire clean energy roots by high energy reformation efficacy and low ecological pollution. Recent studies indicate that these Pd-based bimetallic materials' electrocatalytic performances are improved compared to pure Pd-based materials [26,27].

The Au-Pd NPs showed better catalytic activity than their comparable monometallic counterparts, viz., AuNPs and PdNPs, prepared under similar conditions. The activation energy conditions of the Au-Pd NP-doped graphite conductors are lower, offering them as probable anode materials in basic media-based MeOH FCs at environmental conditions [28–30]. FCs are attractive proton exchange membranes (PEMs), including PEMFCs and DMFCs, and have been known to designate a possible energy source of alternative energy because of their cleanliness and better activity, the reusability of exhaustion heat, and their compliance for mobile, transport, and stationary uses. Current ion efforts into PEMFCs and DMFCs focus on constructing profitable, stable, high-performance FC ingredients to understand their possible wide-ranging industrializations. At the cathode electrodes, Pt nanoparticles based on porous carbons (Pt/C) are usually the catalyst of high-quality [31–33]. The MOR studies inveterate that the presence of Au and Sn in Pt-based catalysts ultimately quantified their possibility to overwhelmed the price of Pt content desired for this application, explaining the purpose of Au in attractive current/potential performance and suggesting the consequence of supportive matrices [34–36]. Further, the electrocatalytic performance of DMFCs towards MOR can be enhanced by decreasing the amount of Pd with the incorporation of conductive polymers. These electroactive conductive polymers are inexpensive, have excellent physicochemical characteristics, and are easy to produce. Incorporating conductive polymers with Pd as an electrocatalyst enhances its redox properties with unique features like higher stability, superior electrocatalytic performance, and strong attachment/or adherence with the electrode surface. By considering these concepts, Using an electrodeposition approach, Chen et al. [37] fabricated a conductive polymer-based nanocomposite, i.e., poly (N-methylthionine)/polyaniline. This nanocomposite shows enhanced electroactivity and electrocatalytic performance toward MOR in DMFCs.

Further, it was also reported that the change in the electronic structure of conductive polymers in the presence of conjugated materials may also enhance the electrocatalytic performance as is done in the case of poly (N-methylthionine)/ electrochemically reduced graphene oxide composite [38]. Similarly, incorporating Pd nanoparticles with polyaniline and poly-diphenylamine copolymer to form a nanocomposite also shows excellent electrocatalytic performance toward MOR and ethanol oxidation reaction in an alkaline medium [39].

Otto Fuel II is an oily liquid with a distinctive smell and a reddish-orange colour used as fuel in torpedo and other weaponry systems by the United States Navy. The Otto Fuel II component consists of propylene glycol dinitrate (76 %), the primary explosive part, dibutyl sebacate (22.5 %), and 2-nitro-phenylamine (1.5 %) [40]. When this material enters into the environment by Naval activity, it affects the environment badly and human health by leaving its toxic effect. So, the removal of the Otto Fuel II component is required. It was previously done by using anaerobic bacterial degradation. With the advancement in science, some conductive polymer-based nanocomposites are also used to remove Otto Fuel II components as described in the present study.

Here, the proposed work has confirmed the successful formation of a 2*ADPA* support material enriched with graphene oxide (GO) and palladium nanoparticles (PdNPs) and used to modify a glassy carbon electrode (GCE) surface. The surface and dispersion of the support and modified support material were analyzed with techniques including Fourier Transform Infrared (FTIR) spectroscopy, Transmission Electron Microscopy (TEM) spectroscopy and X-ray Diffraction (XRD). The modified material activity and stability regarding MeOH oxidation in a basic environment were analyzed using electrochemical methods such as cyclic voltammetry (CV), chronoamperometry and electrochemical impedance spectroscopy (EIS). This will help to explain palladium-deposited 2*ADPA* as a possible anode material for an FC application and also useful in the removal of Otto Fuel II component.

2. Experimental section

2.1. Chemicals

In the present study, we used all salts and solvents of analytical grades for performing our laboratory-based experiment without further processing. While if any method is applied anywhere, we have specifically mentioned the same in the required section. All the chemicals and reagents such as Potassium tetrachloropalladate (II) (K_2PdCl_4, $\geq$ 99 %), methanol (MeOH, $\geq$ 99 %), graphite powder (C, $\geq$ 99 %) sodium borohydride ($NaBH_4$, $\geq$ 99 %), 2-nitrodiphenylamine ($C_{12}H_{10}N_2O_2$, $\geq$ 98 %), sodium nitrate ($NaNO_3$, $\geq$ 90 %), potassium permanganate ($KMnO_4$, $\geq$ 99 %; CDH), hydrochloric acid (HCl, $\geq$ 35 %), Urea ((NH_2)$_2$CO, $\geq$ 98 %), phosphoric acid (H_3PO_4 $\geq$ 85 %), sulfuric acid (H_2SO_4, $\geq$ 95 %), hydrogen peroxide (H_2O_2, $\geq$ 50 %; CDH), ultrapure deionized water (dH_2O, D.I., 18.25 MΩ), alumina powder (Al_2O_3, $\geq$ 99 %) and ammonium persulfate (APS, $\geq$ 99 %) were got as of Merck (St. Louis, MO, USA) and utilized deprived of additional decontamination.

2.2. Synthesis processes of materials

2.2.1. Preparation of graphitic carbon-nitride (gCN) and palladium gCN (Pd-gCN)

In a distinctive synthetic process defined within the works, 20 g of urea was straight calcined in a 50 ml pot into a muffle furnace. The vessel was semi-sealed, heated and reserved at the terminal calcination temperature is about ($T = 550\,^{\circ}$C) for 3 h. After cooling, the pale-yellow powders that were consecutively obtained are labelled as *g*CN. The Pd-*g*CN (5.0 mol % of Pd loading) was synthesized using potassium tetrachloropalladate (II) precursor following the single-step borohydride reduction technique at room temperature. A brownish and dark-grey colloidal material was formed by adding palladium salt. The whole reaction was completed underneath environmental conditions for 120

min. Throughout the reaction, a dark brown material was collected at the bottommost of the container. Detailed graphical representation of the gCN and Pd-gCN synthesis process and their further application in removing otto fuel components are shown in Fig. 1.

2.2.2. Synthesis of graphene oxide (GO)

In the synthesis process we have described in our previously published work [21], graphene oxide (GO) was synthesized by using a modified Hummers method, 5 g of graphite mixed with 2.5 g of NaNO$_3$ by adding 108 mL of sulphuric acid and 12 mL of phosphoric acid by continuous stirring for 10 min in an ice bath. To maintain the mixture's temperature below 5 °C, 15 g of KMnO$_4$ is added slowly in the reaction mixture. The mixture is left in an ice bath for 2 h for reaction and then stirred for 60 min before again being stirred in a 40 °C water bath for about 60 min. After that addition of water done by maintaining the temperature constant 98 °C for 60 min. To make the volume of suspension, 400 ml DI water is added. After 5 min, hydrogen peroxide (15 mL) is added. The reaction product was centrifuged and washed with DI water and hydrochloric acid 5 % solution again and again, and product GO was obtained by drying it at 60 °C [38,41,42]. A detailed graphical representation of the GO synthesis process using Hummer's method is shown in Fig. 2.

2.2.3. Preparation of Pd-2ADPA and Pd-2ADPA-GO composite catalyst

Further, in this study, we prepare Pd supported catalyst on 2ADPA (Pd(0)-2ADPA), and Pd(0)-2ADPA incorporated with GO (Pd(0)-2ADPA-GO). The support material, 2ADPA, was synthesized by the monomeric 2-nitrodiphenylamine (2-NDPA), using 0.05 M ammonium persulphate (APS) as an oxidizing agent and Pd-gCN to make 2-NDPA suitable precursor to synthesized 2ADPA. The addition of Pd-gCN makes it suitable for the Otto fuel II component. Further, Pd(0)-2ADPA was synthesized by reducing 2ADPA by slowly adding 0.05 M K$_2$[PdCl$_4$] as the oxidizing mediator. As a result, the formation of the Pd(0)-2ADPA composite takes place.

Pd(0)-2ADPA-GO was fabricated using a GO solution in deionized water (DI). The addition of 2ADPA was done in this solution by continuous stirring for 15–20 min. After that, 0.05 M K$_2$[PdCl$_4$] was added as the precursor of Pd nanoparticles by constant stirring for 10 min. When the solution is thoroughly mixed, then NaBH$_4$ is added as a reducing agent. This results in the formation of PdNPs via reduction from Pd (II) to Pd (0). Leave the mixture undistributed for 3 to 4 h, then filter and dry it. The resulting material is Pd(0)-2ADPA-GO. Simultaneously, we have also prepared polymeric materials, i.e., polymeric 2 aminodiphenylamine (p-2ADPA), using APS from 2ADPA for further electrochemical and XRD analysis.

2.3. Material characterization

Microscopy studies of the manufactured material were completed using JEOL (JEM-2100) TEM tool furnished with a LaB$_6$ electron basis. The material for TEM study was synthesized by putting a small quantity of prepared composite upon a 200-mesh size Cu-grid covered with a lacy carbon film. The XRD patterns were noted on a Philips PAN analytical X' pert PRO X-ray diffractometer functioning at 40 kV utilizing Cu-Kα radiation ($k = 0.1542$ nm) into the diffraction angle range (2θ) from 10° to 90°. An FTIR analysis was completed using a Shimadzu IRAffinity-1. The UV–vis spectrum was measured utilizing a Shimadzu UV-1800 spectrophotometer with a quartz cuvette.

Electrochemical analysis was performed with a Bio-Logic, SP-200 potentiostat associated with a data regulator. A three-electrode scheme was utilized in the experimentation with a glassy carbon electrode (GCE) as the working conductor. In contrast, correspondingly, the Hg/HgO electrode (1 M NaOH) and a Pt-electrode were utilized as the reference and counter electrodes. A few drops of the colloidal substantial were incorporated into the carbon-covered copper lattice for the TEM analysis, and the needed quantity of material was used for the IR study. The residual amount of the synthesized material was dry under vacuum at 60 °C and used for the XRD study. The collected material was also verified
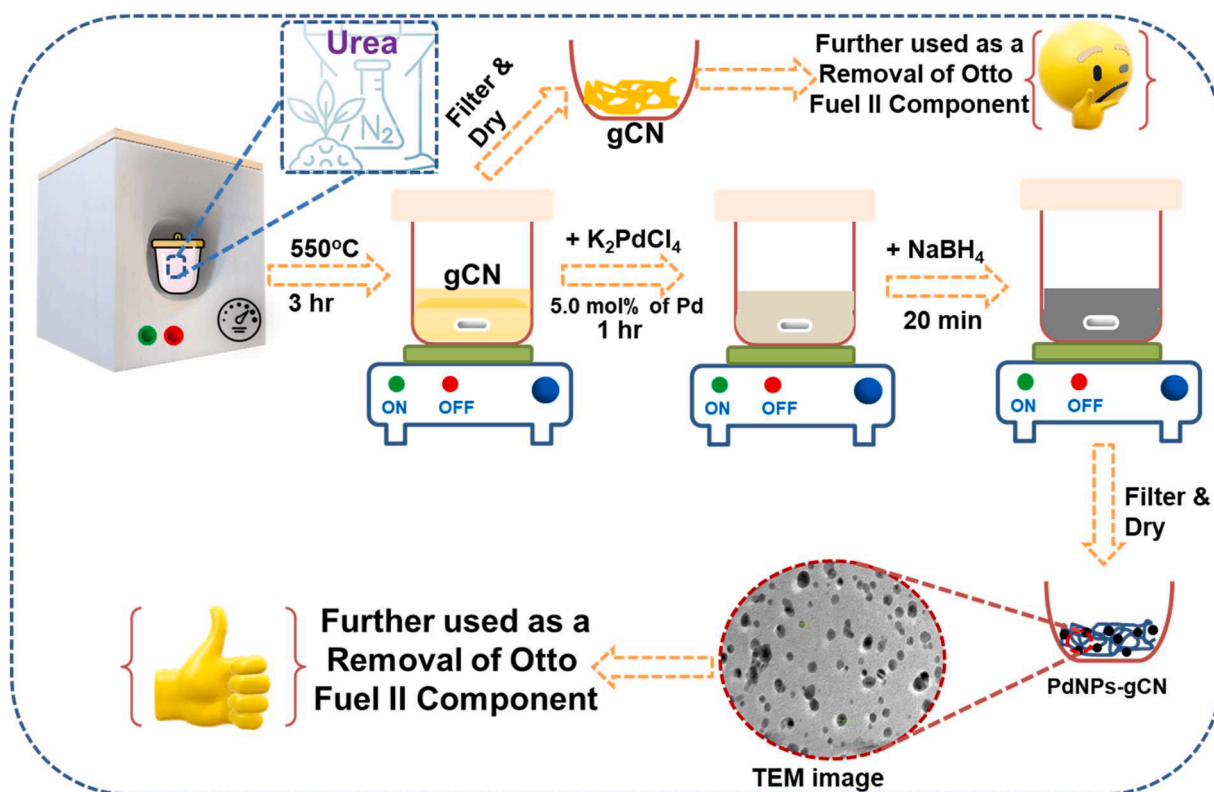

Fig. 1. Synthesis process of gCN and Pd-gCN and their further application in removal of Otto fuel component.
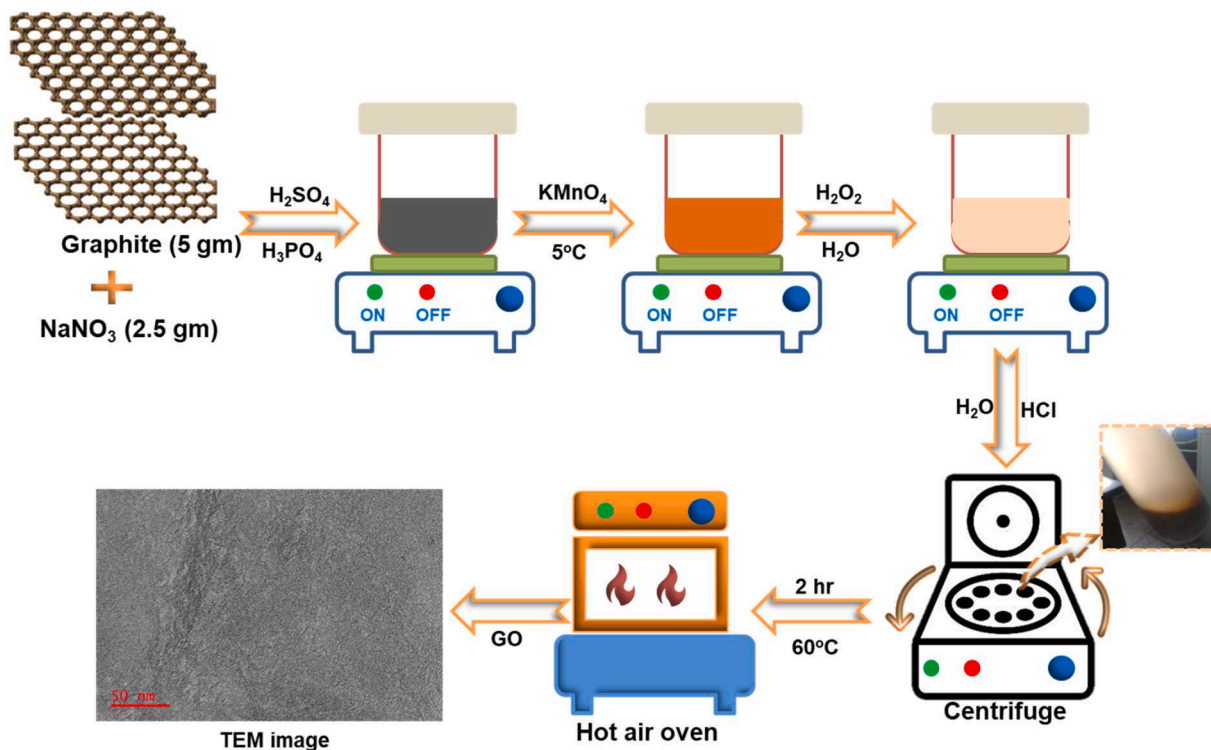
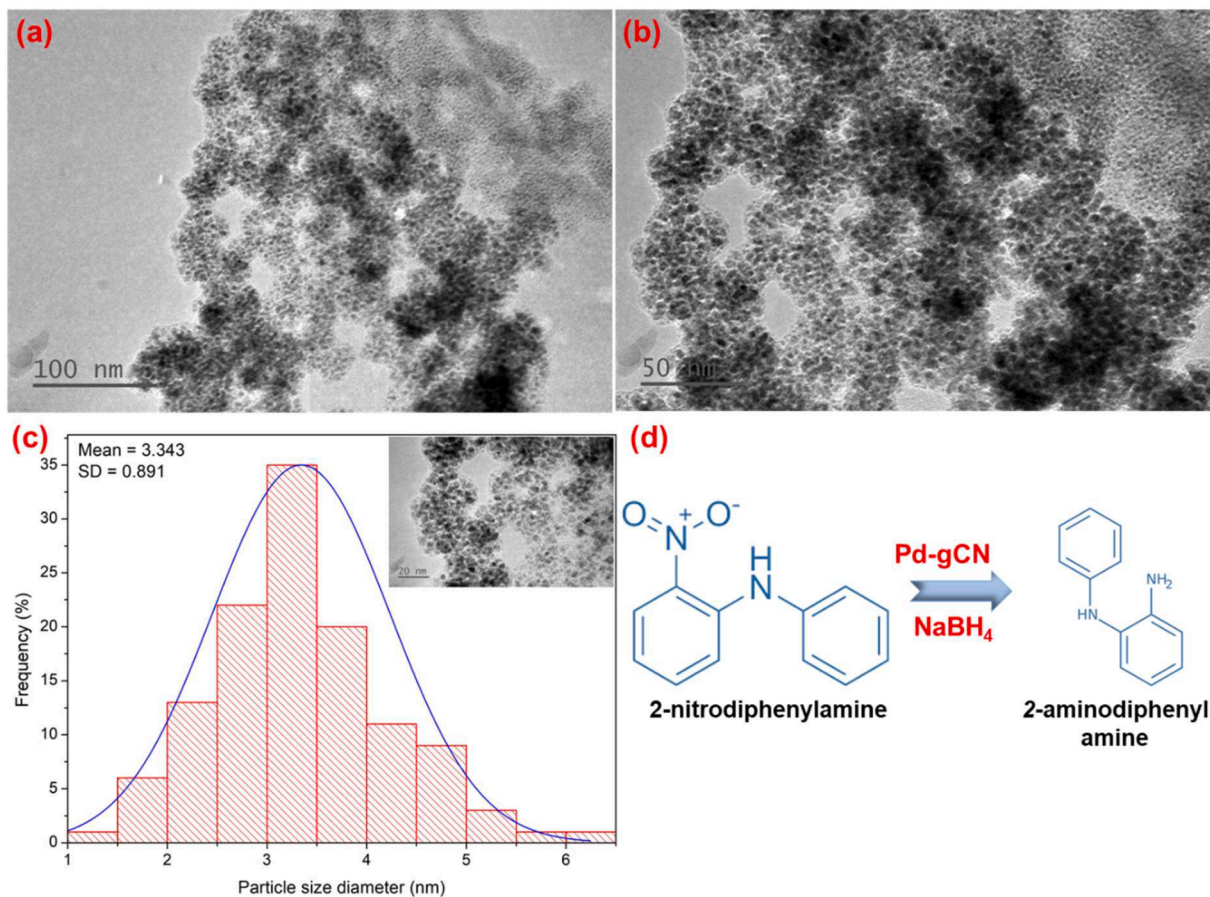**Fig. 2.** Synthesis process of GO using modified Hummer's method.

Fig. 3. (a-c) TEM images at different magnifications and particle size distribution histogram of Pd(0)-*2ADPA*. (d) Schematic representation of the formation of 2ADPA from 2-NDPA in the presence of Pd-gCN.

as an anode material for MOR.

2.4. Electrochemical analysis

A GCE was refined with alumina powder and polished with acetone and DI water, correspondingly. The manufactured materials (gCN, Pd-gCN, GO, Pd(0)-*2ADPA* and Pd(0)-*2ADPA*-GO) were incorporated upon the GCE surface, dry in environmental conditions and utilized for electrochemical studies. For the electro-oxidation analysis of MeOH, the CVs were noted at a sweep rate of 50 mVs^{-1} in a combined solution of KOH (0.5 mol dm^{-3}) and MeOH (1.0 mol dm^{-3}). The electrochemical measurements are done using various techniques like CV, EIS and chronoamperometry (CA).

3. Result and discussion

The preparation of conjugated polymer compressed metal nano-particles (MNPs) has been described utilizing the *in-situ* polymerization and composite formation (IPCF) method [43,44], where MNPs have been fashioned via a one-step reaction and have near interaction among the particles and the polymer via functionalization. This article discusses the results of prepared materials like XRD, UV–vis, FTIR, CV, EIS, and CA in detail.

3.1. Material characterization

Fig. 3(a–c) shows the TEM images and particle size distribution histogram of the as-prepared Pd(0)-*2ADPA* composite's interior structure. The dots present in black indicate the PdNPs doped in the polymeric sheet of *2ADPA*. On high magnification, the increase in density was observed, represented by shady spots. The dark spots indicate that Pd-atoms are present in the nanoscale area. Fig. 3(d) shows the schematic representation of *2ADPA*, demonstrating that 2-NDPA reduced to form *2ADPA* in the presence of Pd-gCN. Further, Pd was reduced into Pd-NPs in the presence of NaBH$_4$ reducing agent to give Pd(0)-*2ADPA* composite.

XRD checks the phase purity of the fabricated material. Fig. 4(a) shows the XRD data of Pd(0)-*2ADPA* and *p-2ADPA*, which was obtained by powder XRD that proves the structural detail of Pd(0) NPs. The XRD pattern shows that a multiple peaks near the value of 2θ around 20° is due to the presence of *p-2ADPA*, while other peaks at 40.7, 45.27 and 66.29° representing the Pd(0), while the broad peaks are due to the small size of particles. The *p-2ADPA* XRD patterns are displayed in Fig. 4 (a). Partial crystallinity was indicated by peaks between 2θ = 10–30°

and a broadband centred at 2θ = 20–30° in the polymer sample [45,46]. Fig. 4(b) shows the XRD of Pd(0)-*2ADPA*-GO. This indicates the presence of PdNPs by its strong peak and GO broad peak near 2θ value of 22.5°. The amorphous nature of GO delivers a high electrochemical surface area for Pd(0)-*2ADPA* for its superior catalytic activity. The XRD peaks of samples shifted toward the higher value angles of 2θ compared to pure Pd-NPs, showing the contraction in the lattice and alloy formation. The crystallite size was calculated using the integral breadth approach from the XRD. This approach is not based on the shape and size of crystal domains [47].

Fig. 5(a) shows the UV–vis spectrum of the polymerization process of 2-NDPA to form *2ADPA* polymer. The spectrum of *2NDPA* (black curve), *2NDPA* with gCN in the absence of reducing agent (red curve), *2NDPA* with gCN in the presence of reducing agent NaBH$_4$ (blue curve and up to 15 min in pink curve) shown in-set. The spectrum of in-set shows that after adding NaBH$_4$ and using gCN to the *2NDPA*, no further intensity has decreased for the next 15 min. This indicates that the reduction of *2NDPA* into *2ADPA* needs to occur more effectively. Fig. 5(a) shows the reduction of *2NDPA* with NaBH$_4$ as an H-source and PdNPs-gCN composite. A broad peak around 435 nm is quenched after the formation of the monomer. The formation of a *2ADPA* monomer indicates a decrease in the *2NDPA* curve due to the removal of the nitro group [48]. The addition of K$_2$[PdCl$_4$] in *2ADPA* starts the polymerization process. The K$_2$[PdCl$_4$] increase the removal rate of monomer; as a result, Pd-NPs are formed. So, a conclusion appears that oxidation of *2ADPA* leads to the reduction of K$_2$[PdCl$_4$]. After adding Pd-NPs, the material shows lower absorbance in the visible region. It was further proved that with the addition of Pd-gCN to the reaction mixture decrease in the intensity is observed, which shows the appearance of monomeric unit *2ADPA*.

Further, with Pd-gCN and NaBH$_4$, a sharp decrease in intensity was observed, which decreases with time; this decrease in intensity with time from 2 min to 3 min shows the reduction of *2NDPA* into *2ADPA* increases and the polymerization of *2ADPA* started with the addition of PdNPs by the gradual decrease in the intensity of the peak. The broad peak that rises slowly near region 470 to 475 nm indicates the formation of quinoids from benzenoids. Fig. 5(b) shows the UV–vis spectrum of *2ADPA* (black curve) and Pd(0)-*2ADPA* (red curve). The spectrum indicates that the intensity of the peak decreases with the addition of PdNPs to the polymer, and absorbance increases as the size of the composite increases.

Raman spectra measure chemical molecules' structure, phase, and morphology with their molecular interaction. Raman spectrum is plotted intensity (count rate) vs Raman shift which is the difference between frequencies of laser light and scattered light by the material and
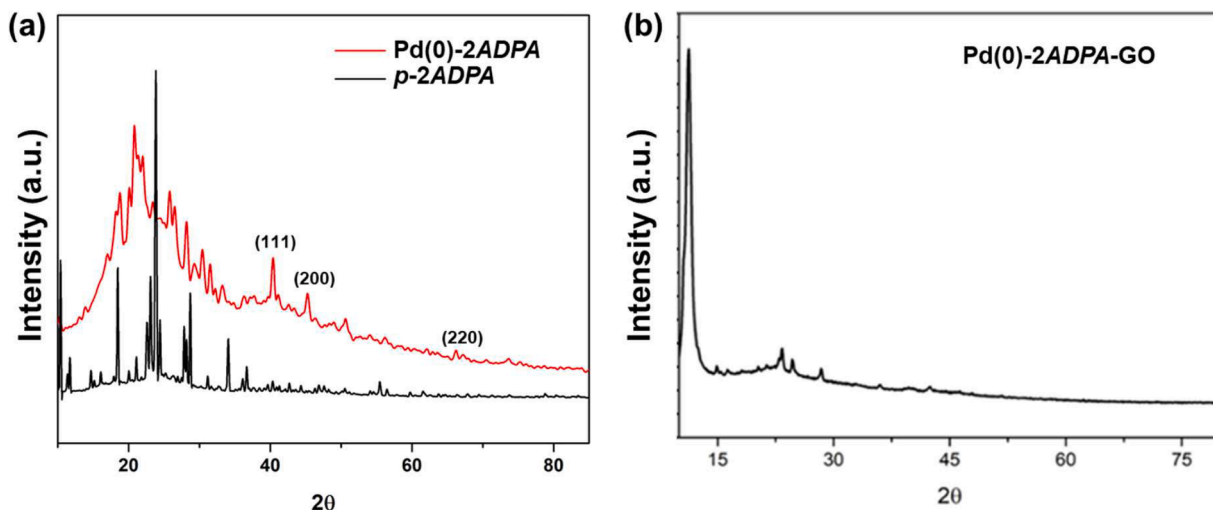

Fig. 4. XRD patterns of (a) Pd(0)-2ADPA and p-2ADPA, (b) Pd(0)-2ADPA-GO.
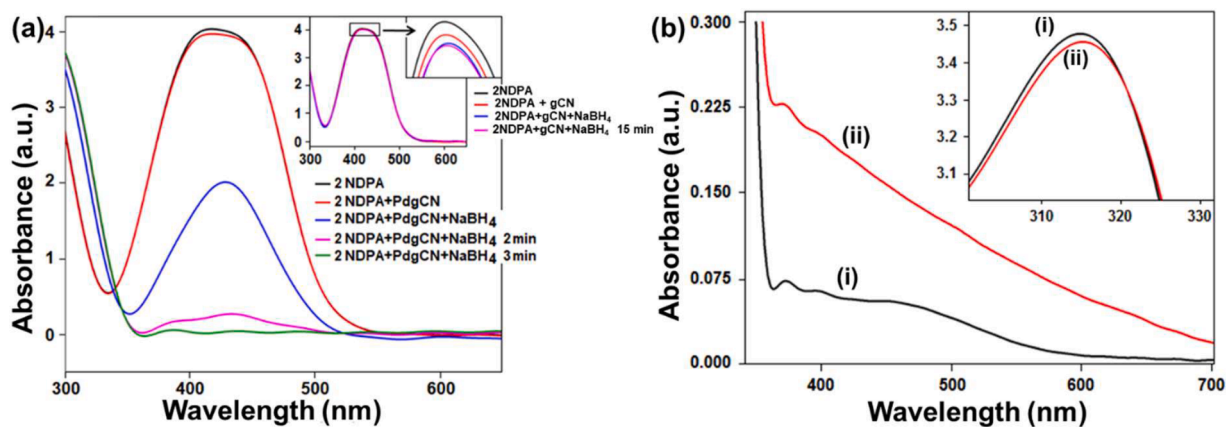
Fig. 5. (a) In-set, the spectrum for 2*NDPA* and the spectra, after the adding of NaBH$_4$ and gCN and no additional reduction in intensity has been recorded of the spectra for subsequent 15 min. In the main figure, the spectrum for 2*NDPA* and after the adding of NaBH$_4$ and Pd-gCN, the steady reduction of intensity of the peak has been recorded (3 min). (b) The UV-visible bands of the 2*ADPA* (i) and Pd(0)-2*ADPA* (ii) composite.

represented as wavenumber. As the particle size increases, the Raman intensity decreases, as shown in Fig. 6(a) for Pd(0)-2*ADPA* composite.

FTIR is used to know about the optical nature of 2*ADPA* and Pd(0)-2*ADPA* materials. The FTIR diagrams are superimposed for comparing pure and polymer-metal doped materials. Fig. 6(b) shows the curves of FTIR for 2*ADPA* (black) and Pd(0)-2*ADPA* (red) with its corresponding peaks. Approx. at 3400 cm^{-1}, a broad peak indicates the stretching of NH that shows the amine group's presence. A peak near 2991 cm^{-1} indicates the single-bonded amine with the N—H bond. In the doped material, this peak is also visible. The stretching of the quinoid appears around 1645 cm^{-1}, and for CN, it is at 1439 cm^{-1}. This peak comes at a lower wavenumber value when the nitro group conjures with the benzene ring. The formation of N$_2$ is a group of two bands near 1645 cm^{-1} and 1439 cm^{-1}. Near 1109 cm^{-1} and 1040 cm^{-1}, the bending vibration of the organic C—H plane is observed. After that, when metal is added to the polymer, the metal-nitrogen bond shortens, resulting in the red shift [49]. The spectrum of Pd(0)-2*ADPA* shows clear peaks at 1017, 1645.48, 2123.75, 2837.80, 2951.07 cm^{-1}, and a broad peak at 3191 to 3600 cm^{-1} that indicates the formation of Pd-Nitrogen interaction in Pd (0)-2*ADPA*. This FTIR spectrum further indicates that NPs of Pd present in a chain-like arrangement that specifically intensifies the spectrum. This is also proved by the TEM study that shows the presence of PdNPs in polymer chain ions of nanoscale size.

3.2. Electrochemical studies

3.2.1. Cyclic voltammetry

To know molecules' reduction and oxidation processes, CV is done. It is a type of potentiodynamic measurement and is done by using a potentiostat. The graph is potential (E) vs current (i), known as a voltammogram. CV provides information about the electrochemically active surface area and interaction of the catalyst with the electrolyte [50]. In CV, the existing is analyzed by sweeping the potential back and forth between adjusted limits. From the voltammogram, materials' reduction and oxidation peaks were obtained that give the material's oxidative and reductive potential. A slope is obtained as a result of CV. For the forward scan, a positive slope indication is obtained. At the same time, the potential is swapped after the first half-cycle, followed by a negative slope, reversing the voltammogram's nature for the second (next) half-cycle [51]. Fig. 7(P(A)) shows the CV of bare GCE (curve 'a'), *polymeric 2-aminodiphenylamine* (*p-2ADPA*) doped GCE (curve 'b') without MeOH and bare GCE (curve 'c'), *p-2ADPA* doped GCE (curve 'd') with 1 M MeOH, in 0.5 M KOH with the potential range −0.8 V to 0.2 V at a scan rate of 50 mV/s. The current density (CD) is maximum in the case of *p-2ADPA-modified* GCE in the presence of MeOH (1 M), i.e., 0.58 mA/cm^2. This is because the presence of MeOH provides more protons and more electrons for the transfer of ions; as a result, CD increases.

Further, Fig. 7(P(B)) shows the CV of Pd(0)-2*ADPA* doped GCE (curve 'e') without and Pd(0)-2*ADPA* doped GCE (curve 'f') with 1 M
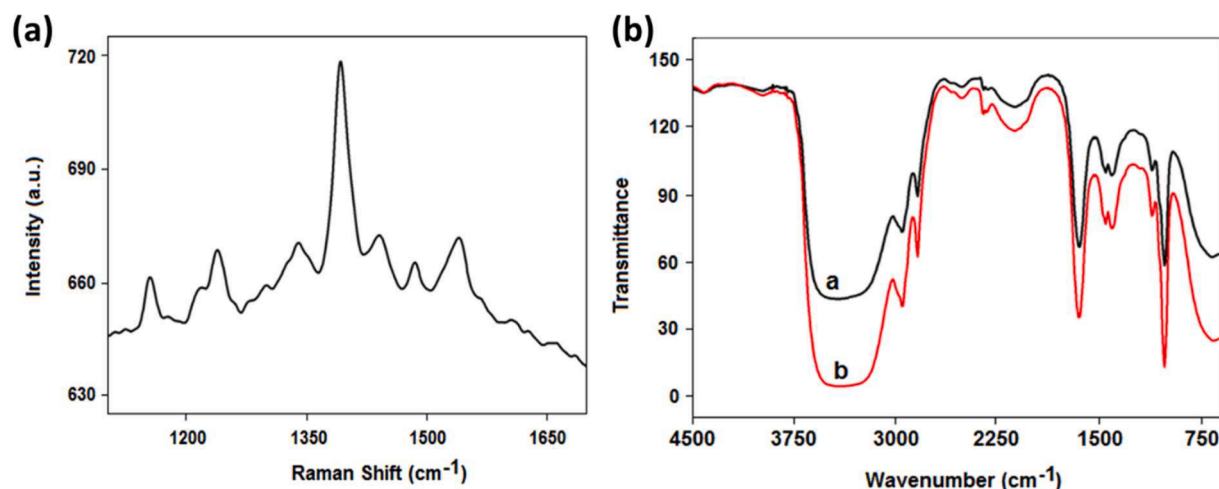

Fig. 6. (a) Raman spectra of Pd(0)-2*ADPA* composite, (b) FTIR spectra of 2*ADPA* (a) and Pd(0)-2*ADPA* (b)
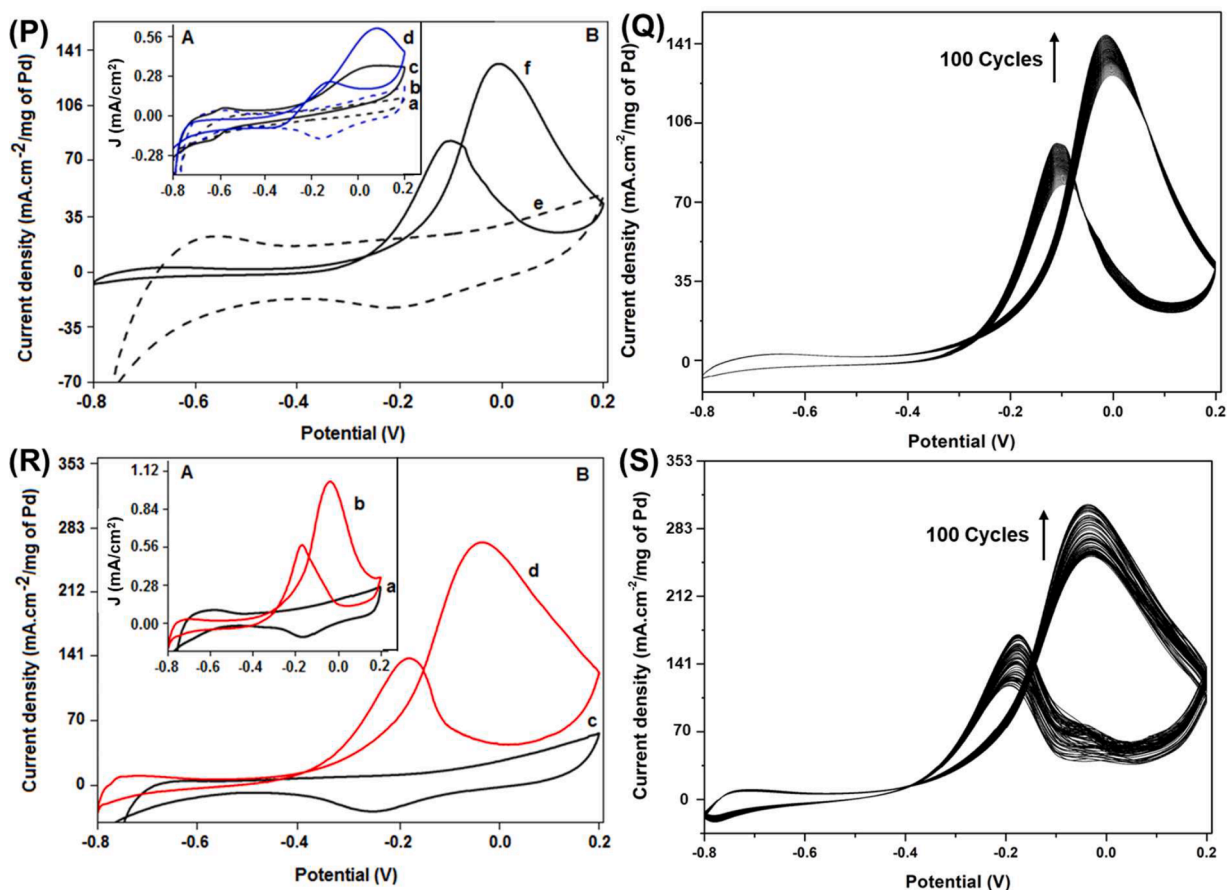
Fig. 7. (P) (A) CV of bare GCE (curve 'a'), *p-2ADPA* doped GCE (curve 'b') without MeOH and bare GCE (curve 'c'), *p-2ADPA* doped GCE (curve 'd') with 1 M MeOH, in 0.5 M KOH. (B) CV of Pd(0)-*2ADPA* doped GCE (curve 'e') without and Pd(0)-*2ADPA* doped GCE (curve 'f') with 1 M MeOH in 0.5 M KOH. Pd(0)-*2ADPA*, I_f/I_b = 1.593. (Q) CV of Pd(0)-*2ADPA* doped GCE signifies the decreasing CD value with every scan with 1 M MeOH in 0.5 M KOH and scan rate: 50 mV/s. Pd(0)-*2ADPA*, I_f/I_b = 1.501. (R) (A) CV of GO doped GCE (curve 'a') without MeOH and GO doped GCE (curve 'b') with of 1 M MeOH, in 0.5 M KOH. (B) CV of Pd(0)-*2ADPA*-GO modified GCE (curve 'c') without and Pd(0)-*2ADPA*-GO modified GCE (curve 'd') with of 1 M MeOH in 0.5 M KOH. Pd(0)-*2ADPA*-GO, I_f/I_b = 1.92. (S) CV of Pd(0)-*2ADPA*-GO doped GCE signifies the increasing CD value with every scan without 1 M MeOH in 0.5 M KOH and scan rate: 50 mV/s. Pd(0)-*2ADPA*-GO, I_f/I_b = 1.74.

MeOH in 0.5 M KOH. Pd(0)-*2ADPA*, having forward and backward current ratio, i.e., I_f/I_b = 1.593. The CD of Pd(0)-*2ADPA* found more in MeOH (1 M) presence, i.e., 132.27 mA/cm^2/mg of Pd. The presence of catalyst Pd also increase the CD as it provides a large electrochemically active surface area for the electro-oxidation of MeOH. Fig. 7(Q) shows the CV of Pd(0)-*2ADPA* modified GCE for 100 cycles represents the decreasing CD value with every scan rate from 145.73 mA/cm^2/mg of Pd to 97.563 mA/cm^2/mg of Pd, in the presence of 1 M MeOH in 0.5 M KOH and a scan rate of 50 mV/s. For Pd(0)-*2ADPA*, I_f/I_b = 1.501. Fig. 7 (R(A)) shows the CV of graphene oxide (GO) doped GCE (curve 'a') without MeOH and GO modified GCE (curve 'b') in the presence of 1 M MeOH in 0.5 M KOH. The GO exhibited a more CD of 1.055 mA/cm^2 in the case of MeOH for the same reason. When GO is combined with Pd(0)-*2ADPA*, it further enhances the CD by increasing the electrooxidation of MeOH. Here, GO stabilizes and improves the material's electric conductivity and CD. In addition, GO provides excellent dispersity and a substantial effective surface area for the supported catalysts [52]. By the addition of GO, the CD increases further as compared to Pd(0)-*2ADPA*, and for Pd(0)-*2ADPA*-GO in the presence of MeOH is found to be 267.94 mA/cm^2/mg of Pd as shown in Fig. 7(R (B)) by curve 'd'. Further, Fig. 7 (S) shows the CV of Pd(0)-*2ADPA*-GO modified GCE signifies the increasing CD value with every scan with 1 M MeOH in 0.5 M KOH and scan rate: 50 mV/s from 308.65 (I_f) to 171.79 (I_b) mA/cm^2/mg of Pd. For the Pd(0)-*2ADPA*-GO, the ratio of I_f/I_b = 1.74.

Fig. 8 shows the CV of GO-doped GCE represents the increasing CD value of 1.25 mA/cm^2 with every scan with 1 M MeOH in 0.5 M KOH
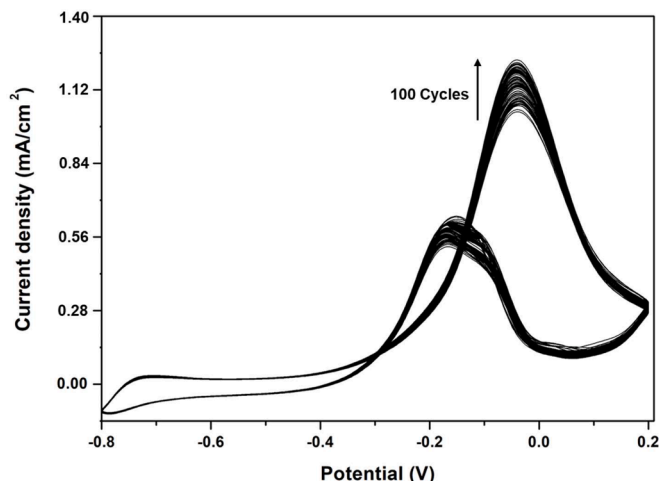
Fig. 8. CV of GO-modified GCE signifies the cumulative CD value with every scan with 1 M MeOH in 0.5 M KOH and scan rate: 50 mV/s. GO, I_f/I_b = 1.92.

with a scan rate of 50 mV/s. For GO, I_f/I_b = 1.92. It is clear from the above discussion that the tolerance power of catalysts for the poisoning species, like adsorbed CO intermediates produced in the electrooxidation of MeOH, is highly based upon the ratio of the forward anodic peak current (I_f) to the backward cathodic peak current (I_b), i.e.,

I_f/I_b. Hence, much efficient removal of the poisoning moieties on the catalyst's surface is due to the higher value of I_f/I_b ratio [53]. This ratio is found higher in the case of catalyst Pd(0)-*2ADPA*-GO, i.e., 1.94 in the presence of MeOH (1 M) in KOH (0.5 M) with higher catalytic performance and more CO tolerance in the MOR.

The CV results of various conductive polymer-based electrocatalysts towards MOR are compared in Table 1.

3.2.2. Electrochemical impedance spectroscopy

EIS is an effective technique for knowing the properties of materials and electrode reactions. EIS provides information about the electrochemical process at the electrode and electrolyte interface in a single measurement. The EIS generally represents in the form of a Nyquist plot. In this imaginary part of impedance data plotted versus the real part [64]. The plot shows the value of charge transfer resistance (R_{CT}) that decreases with the doping, and hence the value of current increases [65]. The EIS analysis done for the as-prepared materials and Nyquist plot shown in Fig. 9 for the (a) *p*-2ADPA, (b) Pd(0)-*2ADPA*, (c) GO and (d) Pd(0)-*2ADPA*-GO in 0.5 M KOH within the frequency range from 3 MHz to 10 kHz. The magnified portion of the Nyquist plot shown is inset which shows the value of R_{CT} for different materials. It was found that the value of R_{CT} was lowest for Pd(0)-*2ADPA*-GO, i.e., 10.16 ohm with a higher current value. While the other materials have a value of R_{CT} are 515.06 ohms for *p*-2ADPA, 57.36 ohms for Pd(0)-*2ADPA*, and 238.79 ohms for GO. The result showed that doping of polymer with Pd and GO decreases the value of R_{CT}; hence performance of material for electro-oxidation of MeOH increases with a higher current value.

3.2.3. Chronoamperometry

The investigation of the strength and stability of various prepared electrocatalyst CA was done. It is done to measure current-time dependence during electrooxidation reactions that occur at the electrode. Here CA was used to examine the electrooxidation of MeOH on modified GCE with catalyst GO, Pd(0)-*2ADPA* and Pd(0)-*2ADPA*-GO in 1.0 M MeOH and 0.5 M KOH at a potential of -0.04 V, -0.007 V and -0.035 V vs Hg/HgO respectively for 3000 s. As shown in Fig. 10, it is found that the CD of Pd(0)-*2ADPA*-GO is higher and more durable compared to other catalysts, i.e., Pd(0)-*2ADPA* and GO. The order of CD is Pd(0)-*2ADPA*-GO >Pd(0)-*2ADPA*>GO>*p*-2ADPA. The catalyst Pd(0)-*2ADPA*-GO exhibited superior electrocatalytic performance towards the electrochemical oxidation of MeOH. A decrease in CD was observed in the case
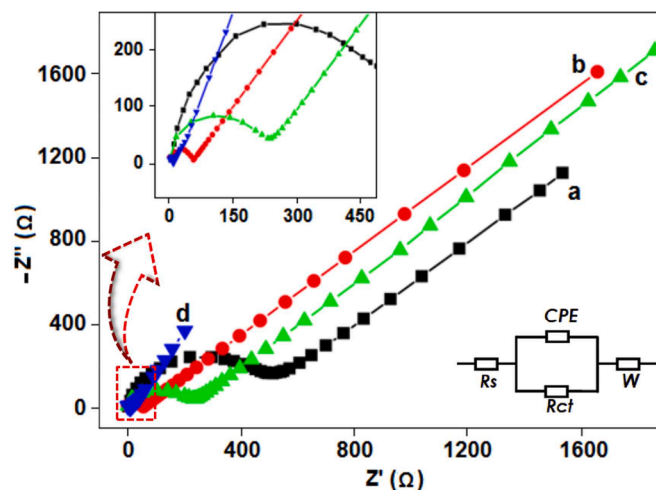

Fig. 9. The EIS analysis for the (a) p-2ADPA, (b) Pd(0)-2ADPA, (c) GO and (d) Pd(0)-2ADPA-GO in 0.5 M KOH within the frequency range from 3 MHz to 10 kHz.
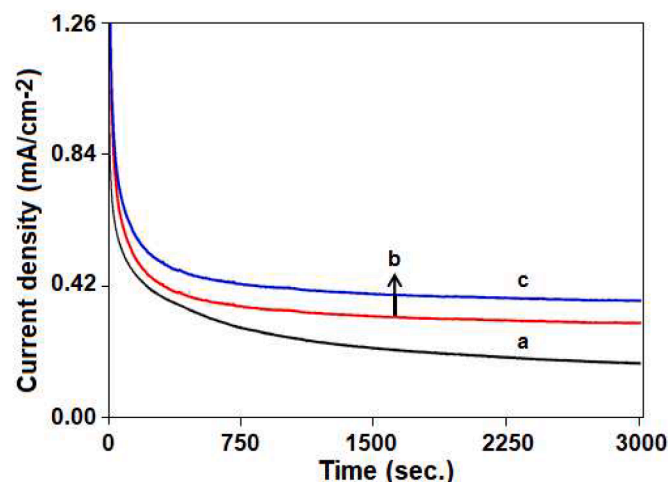

Fig. 10. CA analysis of (a) GO, (b) Pd(0)-2ADPA and (c) Pd(0)-2ADPA-GO doped GCE with 1 M MeOH in 0.5 M KOH at (a) -0.04, (b) -0.007 and (c) -0.035 V correspondingly for the 3000 s.

of other catalysts except Pd(0)-*2ADPA*-GO. This result is due to the base material's higher exterior area and the corrosion resistance nature in this strong alkaline medium.

4. Conclusion

The current report shows a novel synthesis method of palladium-incorporated functional polymer composite which showed outstanding electrocatalytic activity for MeOH oxidation in a basic solution. The facile synthesis process and the synthesized material's durability and recyclability show that the material could be applied in DMFCs. By comparing the as-prepared catalyst, it is found that all the fabricated catalysts exhibited good catalytic performance, having many active sites with synergistic effects due to the presence of GO as a stabilizer. The CV, EIS, and CA analysis of these catalysts show that catalyst Pd(0)-*2ADPA*-GO modified GCE in the presence of MeOH (1 M) in KOH (0.5 M) shows more tolerance toward CO as compared to other materials, i.e., Pd(0)-*2ADPA*, GO-GCE, *p*-2ADPA-GCE. This Pd(0)-*2ADPA*-GO also exhibited superior catalytic performance toward the electro-oxidation of MeOH because of higher electric conductivity and fast transfer of electrons by GO with the higher CD value 308.65 mA/cm^2/mg of Pd.

Table 1
Electrocatalytic activity of conductive polymer-based composites towards MOR.

Name of composites	Electrolyte used	Current density/ specific activity	I_f/I_b value	References
Pt-Ru/poly(N-vinyl carbazole	H$_2$SO$_4$ (0.5 M)	276 mA/cm^2		[54]
Pt-Sn/Polyaniline (PANI)-Rice husk ash	H$_2$SO$_4$ (0.5 M)	2.983×10^{-3} A/mg	1.38	[55]
Pt-Pd-rGO/PANI	KOH (1 M)	84.93 mA/cm^2	-	[56]
Pd-Au Nanowires	NaOH (0.5 M)	85 mA/cm^2	-	[57]
Pd/Cu$_3$P/rGO	KOH (1 M)	33.9 mA/cm^2	-	[58]
Pt nanocube assemblies/PANI	HClO$_4$ (0.1 M)	0.85 mA/cm^2	-	[59]
PtPd/Polypyrrole (Ppy)/PtPd	H$_2$SO$_4$ (0.5 M)	≈ 0.92 mA/cm^2	-	[60]
Pt$_{66}$Pd$_{34}$/PPy	KOH (0.1 M)	9.52 mA /cm^2	-	[61]
Pt$_{24}$Pd$_{26}$Au$_{50}$/PPy	KOH (0.1 M)	6.76 mA /cm^2	-	[61]
Pd nanoflowers /PPy/ multi walled carbon nanotubes	KOH (0.5 M)	1.69 mA /cm^2		[62]
Pd-graphitic carbon nitride/PANI	KOH (0.5 M)	$\approx 3.74 \times 10^{-3}$ A/cm^2	-	[63]
Pd(0)-*2ADPA*-GO	KOH (0.5 M)	308.65 mA/ cm^2/mg$_{Pd}$	1.74	This work

CRediT authorship contribution statement

Kirti Mishra: Data curation, Formal analysis, Writing – original draft. **Nishu Devi:** Data curation, Formal analysis, Software, Visualization. **Samarjeet Singh Siwal:** Conceptualization, Funding acquisition, Validation, Resources, Supervision, Writing – review & editing. **Vijay Kumar Thakur:** Validation, Resources, Funding acquisition, Supervision, Writing – review & editing.

Declaration of competing interest

The authors declare that they have no known competing financial interests or personal relationships that could have appeared to influence the work reported in this paper.

Data availability

Data will be made available on request.

Supplementary materials

Supplementary material associated with this article can be found, in the online version, at doi:10.1016/j.surfin.2024.104015.

References

[1] Y. Cui, J. Zhang, G. Zhang, J. Huang, P. Liu, M. Antonietti, X. Wang, Synthesis of bulk and nanoporous carbon nitride polymers from ammonium thiocyanate for photocatalytic hydrogen evolution, J. Mater. Chem. 21 (2011) 13032–13039.

[2] S.S. Siwal, H. Kaur, R. Deng, Q. Zhang, A review on electrochemical techniques for metal recovery from waste resources, Curr. Opin. Green. Sustain. Chem. 39 (2023) 100722.

[3] A.K. Rana, E. Mostafavi, W.F. Alsanie, S.S. Siwal, V.K. Thakur, Cellulose-based materials for air purification: a review, Ind. Crop. Prod. 194 (2023) 116331.

[4] X. Li, J. Wei, Y. Chai, S. Zhang, Carbon nanotubes/tin oxide nanocomposite-supported Pt catalysts for methanol electro-oxidation, J. Colloid. Interface Sci. 450 (2015) 74–81.

[5] K. Sheoran, H. Kaur, S.S. Siwal, V.K. Thakur, Dual role is always better than single: ionic liquid as a reaction media and electrolyte for carbon-based materials in supercapacitor applications, Adv. Energy Sustainab. Res. (2023) 2300021 n/a.

[6] H. Kaur, S.S. Siwal, R.V. Saini, N. Singh, V.K. Thakur, Significance of an electrochemical sensor and nanocomposites: toward the electrocatalytic detection of neurotransmitters and their importance within the physiological system, ACS. Nanosci. Au 3 (2023) 1–27.

[7] S.S.M.a.J. Datta, Characterization of Pt-Pd/C electrocatalyst for methanol oxidation in alkaline medium, Int. J. Electrochem. (2011) 16, 2011.

[8] C. Lamy, E.M. Belgsir, J.M. Léger, Electrocatalytic oxidation of aliphatic alcohols: application to the direct alcohol fuel cell (DAFC), J. Appl. Electrochem. 31 (2001) 799–809.

[9] C. Hu, X. Wang, Highly dispersed palladium nanoparticles on commercial carbon black with significantly high electro-catalytic activity for methanol and ethanol oxidation, Int. J. Hydrog. Energy 40 (2015) 12382–12391.

[10] E. Antolini, Palladium in fuel cell catalysis, Energy Environ. Sci. 2 (2009) 915–931.

[11] K. Mishra, N. Devi, S.S. Siwal, V.K. Thakur, Insight perspective on the synthesis and morphological role of the noble and non-noble metal-based electrocatalyst in fuel cell application, Appl. Catal.: B: Environ. 334 (2023) 122820.

[12] K. Mishra, N. Devi, S.S. Siwal, Q. Zhang, W.F. Alsanie, F. Scarpa, V.K. Thakur, Ionic liquid-based polymer nanocomposites for sensors, energy, biomedicine, and environmental applications: roadmap to the future, Adv. Sci. 9 (2022) 2202187.

[13] C.L. Vecchio, X. Lyu, I. Gatto, B. Zulevi, A. Serov, V. Baglio, C.L. Vecchio, I. Gatto, V. Baglio, Performance investigation of alkaline direct methanol fuel cell with commercial PGM-free cathodic materials, J. Power. Source. 561 (2023) 232732.

[14] Y. Chen, S. Zhang, J. Chung-Yen Jung, J. Zhang, Carbons as low-platinum catalyst supports and non-noble catalysts for polymer electrolyte fuel cells, Prog. Energy Combust. Sci. 98 (2023) 101101.

[15] L. Zhang, J. Zhang, W. Tan, C. Zhong, Y. Tu, H. Song, L. Du, S. Liao, Z. Cui, Amorphous TiO_x stabilized intermetallic Pt_3Ti nanocatalyst for methanol oxidation reaction, Nano Lett. 23 (2023) 5187–5193.

[16] S. Zhao, T. Wang, Z. Ji, Y. Song, Y. Li, J. Liu, W. Hu, Spatial decoupling of dehydrogenation and CO oxidation by Ni-Co-Ti hierarchical trimetallic catalyst for electrocatalytic oxidation of methanol, Appl. Cataly. B: Environ. 320 (2023) 122024.

[17] S.S. Siwal, Q. Zhang, N. Devi, K.V. Thakur, Carbon-based polymer nanocomposite for high-performance energy storage applications, Polym. (Basel) 12 (2020).

[18] S.S. Siwal, S. Thakur, Q.B. Zhang, V.K. Thakur, Electrocatalysts for electrooxidation of direct alcohol fuel cell: chemistry and applications, Mater. Today Chem. 14 (2019) 100182.

[19] S. Samarjeet, G. Sarit, N. Debkumar, D. Nishu, K.P. Venkata, B. Rasmita, M. Kaushik, Synergistic effect of graphene oxide on the methanol oxidation for fuel cell application, Mater. Res. Express. 4 (2017) 095306.

[20] S.S. Siwal, Q. Zhang, C. Sun, V.K. Thakur, Graphitic carbon nitride doped copper–manganese alloy as high–performance electrode material in supercapacitor for energy storage, Nanomaterials 10 (2019).

[21] S. Siwal, N. Devi, V. Perla, R. Barik, S. Ghosh, K. Mallick, The influencing role of oxophilicity and surface area of the catalyst for electrochemical methanol oxidation reaction: a case study, Mater. Res. Innov. (2018) 1–8.

[22] Q. Su, J. Sun, J. Wang, Z. Yang, W. Cheng, S. Zhang, Urea-derived graphitic carbon nitride as an efficient heterogeneous catalyst for CO2 conversion into cyclic carbonates, Catal. Sci. Technol. 4 (2014) 1556–1562.

[23] M. Roca-Ayats, G. García, J.L. Galante, M.A. Peña, M.V. Martínez-Huerta, TiC, TiCN, and TiN supported Pt electrocatalysts for CO and methanol oxidation in acidic and alkaline media, J. Phys. Chem. C 117 (2013) 20769–20777.

[24] N. Devi, S.S. Siwal, V.K. Perla, S.K. Ghosh, K. Mallick, Promotional role of gold in electrochemical methanol oxidation, Cataly. Struct. Reactiv. 5 (2019) 1–9.

[25] F. Su, Z. Tian, C.K. Poh, Z. Wang, S.H. Lim, Z. Liu, J. Lin, Pt nanoparticles supported on nitrogen-doped porous carbon nanospheres as an electrocatalyst for fuel cells, Chem. Mater. 22 (2010) 832–839.

[26] P. Xi, Y. Cao, F. Yang, C. Ma, F. Chen, S. Yu, S. Wang, Z. Zeng, X. Zhang, Facile synthesis of Pd-based bimetallic nanocrystals and their application as catalysts for methanol oxidation reaction, Nanoscale 5 (2013) 6124–6130.

[27] F. Li, X. Chang, S. Wang, Y. Guo, H. Li, K. Wu, Excellent electrocatalytic performance toward methanol oxidation of hierarchical porous NiCu obtained by electrochemical dealloying, J. Alloy. Compd. 934 (2023) 167811.

[28] A. Renjith, V. Lakshminarayanan, One step preparation of "ready to use" Au@Pd nanoparticle modified surface using deep eutectic solvents and a study of its electrocatalytic properties in methanol oxidation reaction, J. Mater. Chem. A 3 (2015) 3019.

[29] S. Siwal, M. Choudhary, S. Mpelane, R. Brink, K. Mallick, Single step synthesis of a polymer supported palladium composite: a potential anode catalyst for the application of methanol oxidation, RSC. Adv. 6 (2016) 47212–47219.

[30] S. Siwal, S. Matseke, S. Mpelane, N. Hooda, D. Nandi, K. Mallick, Palladium-polymer nanocomposite: an anode catalyst for the electrochemical oxidation of methanol, Int. J. Hydrog. Energy 42 (2017) 23599–23605.

[31] W. Yang, Q. Zhang, S.S. Siwal, Y. Hua, C. Xu, Dynamic structure evolution of free-standing S-doped porous Co-Fe microspheres with enhanced oxygen evolution electrocatalysis in alkaline media, Electrochim. Acta (2020) 137038.

[32] J. Zeng, J. Liu, S.S. Siwal, W. Yang, X. Fu, Q. Zhang, Morphological and electronic modification of 3D porous nickel microsphere arrays by cobalt and sulfur dual synergistic modulation for overall water splitting electrolysis and supercapacitors, Appl. Surf. Sci. (2019).

[33] K. Kwon, Y.J. Sa, J.Y. Cheon, S.H. Joo, Ordered mesoporous carbon nitrides with graphitic frameworks as metal-free, highly durable, methanol-tolerant oxygen reduction catalysts in an acidic medium, Langmuir 28 (2012) 991–996.

[34] B. Singh, L. Murad, F. Laffir, C. Dickinson, E. Dempsey, Pt based nanocomposites (mono/bi/tri-metallic) decorated using different carbon supports for methanol electro-oxidation in acidic and basic media, Nanoscale 3 (2011) 3334–3349.

[35] V. Baglio, R.S. Amin, K.M. El-Khatib, S. Siracusano, C. D'Urso, A.S. Arico, IrO_2 as a promoter of Pt-Ru for methanol electro-oxidation, Phys. Chem. Chem. Phys. 16 (2014) 10414–10418.

[36] H. Lei, X. Li, C. Sun, J. Zeng, S.S. Siwal, Q. Zhang, Galvanic replacement–mediated synthesis of Ni-supported Pd nanoparticles with strong metal–support interaction for methanol electro-oxidation, Small. 15 (2019) 1804722.

[37] C. Chen, T. Xu, A. Chen, L. Lu, Y. Gao, Electrosynthesis of Poly(N-methylthionine)/polyaniline nanocomposites with enhanced electrochemical and electrocatalytic activities, J. Electrochem. Soc. 163 (2016) G159.

[38] C. Chen, Z. Gan, K. Zhou, Z. Ma, Y. Liu, Y. Gao, Catalytic polymerization of N-methylthionine at electrochemically reduced graphene oxide electrodes, Electrochim. Acta 283 (2018) 1649–1659.

[39] S.L. Madaswamy, M. Alfakeer, A.A.A. Bahajjaj, M. Ouladsmane, S.M. Wabaidur, C.-x. Chen, R. Dhanusuraman, Remarkable electrocatalytic activity of Pd nanoparticles dispersed on polyaniline-polydiphenylamine copolymer nanocomposite for methanol and ethanol oxidation reaction, Synth. Met. 281 (2021) 116925.

[40] S. Powell, P.D. Franzmann, R. Cord-Ruwisch, S. Toze, Degradation of 2-nitrodi-phenylamine, a component of Otto fuel II, by Clostridium spp, Anaerobe 4 (1998) 95–102.

[41] J. Song, X. Wang, C.-T. Chang, Preparation and characterization of graphene oxide, J. Nanomater. 2014 (2014) 276143.

[42] J. Zhao, S. Zhang, X. Ke, A. Pan, Q. Zhou, S. Zeng, P. Chen, Y. Xu, W. Nie, Y. Zhou, Simultaneously tuning interfacial and interlaminar properties of glass fiber fabric/epoxy laminated composites via modifying fibers with graphene oxide, Compos. Sci. Technol. 235 (2023) 109970.

[43] M. Choudhary, S. Siwal, K. Mallick, Single step synthesis of a 'silver-polymer hybrid material' and its catalytic application, RSC. Adv. 5 (2015) 58625–58632.

[44] M. Choudhary, S.K. Shukla, A. Taher, S. Siwal, K. Mallick, Organic–inorganic hybrid supramolecular assembly: an efficient platform for nonenzymatic glucose sensor, ACS. Sustain. Chem. Eng. 2 (2014) 2852–2858.

[45] J. Ding, K.-Y. Chan, J. Ren, F.-s. Xiao, Platinum and platinum–ruthenium nanoparticles supported on ordered mesoporous carbon and their electrocatalytic performance for fuel cell reactions, Electrochim. Acta 50 (2005) 3131–3141.

[46] S. Yang, F. Liao, Characterization and morphology control of poly(p-phenylenediamine) microstructures in different pH, Nano Brief Rep. Rev. 13 (2011) 597–601.

[47] M. Oezaslan, P. Strasser, Activity of dealloyed $PtCo_3$ and $PtCu_3$ nanoparticle electrocatalyst for oxygen reduction reaction in polymer electrolyte membrane fuel cell, J. Power. Source. 196 (2011) 5240–5249.

[48] H. Kaur, K. Sheoran, S.S. Siwal, R.V. Saini, A.K. Saini, W.F. Alsanie, V.K. Thakur, Role of silver nanoparticle-doped 2-aminodiphenylamine polymeric material in the detection of dopamine (DA) with uric acid interference, Mater. (Basel) 15 (2022).

[49] N.H. Rezazadeh, F. Buazar, S. Matroodi, Synergistic effects of combinatorial chitosan and polyphenol biomolecules on enhanced antibacterial activity of biofunctionalized silver nanoparticles, Sci. Rep. 10 (2020) 19615.

[50] S. Li, A. Thomas, Chapter 12 - Emerged carbon nanomaterials from metal-organic precursors for electrochemical catalysis in energy conversion, in: F. Ran, S. Chen (Eds.), Advanced Nanomaterials for Electrochemical-Based Energy Conversion and Storage, Elsevier, 2020, pp. 393–423.

[51] Y.S. Choudhary, L. Jothi, G. Nageswaran, Chapter 2 - electrochemical characterization, in: S. Thomas, R. Thomas, A.K. Zachariah, R.K. Mishra (Eds.), Spectroscopic Methods for Nanomaterials Characterization, Elsevier, 2017, pp. 19–54.

[52] S.J. Hoseini, M. Bahrami, Z. Samadi Fard, S.F. Hashemi Fard, M. Roushani, B. H. Agahi, R. Hashemi Fath, S.S. Sarmoor, Designing of some platinum or palladium-based nanoalloys as effective electrocatalysts for methanol oxidation reaction, Int. J. Hydrog. Energy 43 (2018) 15095–15111.

[53] S.J. Hoseini, M. Bahrami, M. Dehghani, Formation of snowman-like Pt/Pd thin film and Pt/Pd/reduced-graphene oxide thin film at liquid–liquid interface by use of organometallic complexes, suitable for methanol fuel cells, RSC. Adv. 4 (2014) 13796–13804.

[54] J.-H. Choi, K.-W. Park, H.-K. Lee, Y.-M. Kim, J.-S. Lee, Y.-E. Sung, Nano-composite of PtRu alloy electrocatalyst and electronically conducting polymer for use as the anode in a direct methanol fuel cell, Electrochim. Acta 48 (2003) 2781–2789.

[55] D. Prasanna, V. Selvaraj, Pt and Pt-Sn nanoparticles decorated conductive polymer-biowaste ash composite for direct methanol fuel cell, Korea. J. Chem. Eng. 33 (2016) 1489–1499.

[56] R. Arukula, M. Vinothkannan, A.R. Kim, D.J. Yoo, Cumulative effect of bimetallic alloy, conductive polymer and graphene toward electrooxidation of methanol: an efficient anode catalyst for direct methanol fuel cells, J. Alloy. Compd. 771 (2019) 477–488.

[57] Q.-L. Wang, R. Fang, L.-L. He, J.-J. Feng, J. Yuan, A.-J. Wang, Bimetallic PdAu alloyed nanowires: rapid synthesis via oriented attachment growth and their high electrocatalytic activity for methanol oxidation reaction, J. Alloy. Compd. 684 (2016) 379–388.

[58] K. Zhang, Z. Xiong, S. Li, B. Yan, J. Wang, Y. Du, Cu3P/RGO promoted Pd catalysts for alcohol electro-oxidation, J. Alloy. Compd. 706 (2017) 89–96.

[59] X. Sun, N. Zhang, X. Huang, Polyaniline-coated platinum nanocube assemblies as enhanced methanol oxidation electrocatalysts, ChemCatChem. 8 (2016) 3436–3440.

[60] H. Xu, L.-X. Ding, C.-L. Liang, Y.-X. Tong, G.-R. Li, High-performance polypyrrole functionalized PtPd electrocatalysts based on PtPd/PPy/PtPd three-layered nanotube arrays for the electrooxidation of small organic molecules, NPG. Asia Mater. 5 (2013) e69.

[61] S. Ghosh, S. Bera, S. Bysakh, R.N. Basu, Conducting polymer nanofiber-supported Pt alloys: unprecedented materials for methanol oxidation with enhanced electrocatalytic performance and stability, Sustain. Energy Fuel. 1 (2017) 1148–1161.

[62] L. Abolghasemi Fard, R. Ojani, J.B. Raoof, Electrodeposition of three-dimensional Pd nanoflowers on a PPy@MWCNTs with superior electrocatalytic activity for methanol electrooxidation, Int. J. Hydrog. Energy 41 (2016) 17987–17994.

[63] M. Eswaran, R. Dhanusuraman, P.-C. Tsai, V.K. Ponnusamy, One-step preparation of graphitic carbon nitride/Polyaniline/Palladium nanoparticles based nanohybrid composite modified electrode for efficient methanol electro-oxidation, Fuel 251 (2019) 91–97.

[64] S. Wang, J. Zhang, O. Gharbi, V. Vivier, M. Gao, M.E. Orazem, Electrochemical impedance spectroscopy, Nat. Rev. Method. Primer. 1 (2021) 41.

[65] K. Mishra, V. Kumar Thakur, S. Singh Siwal, Graphitic carbon nitride based palladium nanoparticles: a homemade anode electrode catalyst for efficient direct methanol fuel cells application, Mater. Today: Proceed. 56 (2022) 107–111.